Available online at www.sciencedirect.com

ScienceDirect

Advances in Space Research 72 (2023) 309–326

ADVANCES IN SPACE RESEARCH (a COSPAR publication)

www.elsevier.com/locate/asr

Gangotri glacier dynamics from multi-sensor SAR and optical data

Praveen Kumar Thakur [a,*], Anukesh Krishnankutty Ambika [b], Sanjay M. Bisht [a], Alfred Stein [c], Anirudha Mahagaonkar [d], Uday Kumar [a], Vaibhav Garg [a], Varun Khajuria [a], Arpit Chouksey [a], Snehmani [e], Prakash Chauhan [f], SP Aggarwal [g]

[a] *Water Resources Department, Indian Institute of Remote Sensing, Dehradun 248001, Uttarakhand, India*
[b] *Indian Institute of Remote Sensing & University of Twente, Dehradun 248001, Uttarakhand, India*
[c] *Faculty of Geo-Information Science and Earth Observation (ITC), University of Twente, PO Box 217, 7500 AE Enschede, the Netherlands*
[d] *Indian Institute of Remote Sensing, Dehradun 248001, Uttarakhand, India*
[e] *Defense Geoinformatics Research Establishment (DGRE) – 248001, Chandigarh 160036, India*
[f] *National Remote Sensing Centre, Balanagar, Hyderabad, Telangana 500037, India*
[g] *North East Space Application Center, DoS, Umiam 793103, Meghalaya, India*

Received 6 December 2021; received in revised form 27 February 2023; accepted 1 March 2023
Available online 8 March 2023

Abstract

The present study has analyzed dynamics of Gangotri glacier using multiple remote sensing (RS) datasets and ground based observations. Interferometric Synthetic Aperture Radar (InSAR) data pairs from European Remote Sensing satellite (ERS 1/2) tandem pair for spring of 1996, Sentinel-1 SAR pairs and Japanese's Advance Land Observation System (ALOS) PALSAR-2 SAR data for Spring of 2015 were used to derive glacier-surface velocity at seasonal time scale using Differential InSAR (DInSAR) techniques. Bi-static TanDEM-X (Experimental) data was used for the 1st time to estimate glacier surface elevation changes for a period of 22, 44, 88 days during summer of 2012 using InSAR techniques in this study. Annual glacier velocity was also estimated using temporal panchromatic data of LANDSAT-5 (30 m), LANDSAT-7/8 (15 m), Sentinel-2 (10 m) and Indian Remote Sensing Satellite IRS-1C/1D panchromatic (5 m) data during 1998–2019 with feature tracking approach. This study has estimated glacier surface velocity and surface elevation changes for the major parts of Gangotri glacier and its tributary glaciers using medium to high resolution optical and SAR datasets, at annual and seasonal time scale, which is an improvement over earlier studies, wherein snout based glacier recession or only main glacier velocities were reported. The velocity and slope were used to assess glacier-ice thickness distribution using Glabtop-2, slope dependent and laminar flow based methods over the Gangotri group of glaciers. The estimated ice thickness was estimated in the range of 58–550 m for the complete glacier while few small areas in middle & upper regions carry higher thickness of about 607 m. The estimated glacier-ice thickness was found in the range of 58–67 m at the snout region. The estimation was validated using 2014 field measurements from Terrestrial Laser Scanner (TLS) for the first time and correlation was found to be 0.799 at snout of the glacier.

Keywords: Gangotri glacier; Sentinel-1; Landsat; Elevation changes; IRS; Tandem-x

1. Introduction

The Himalayan region has one of the largest glacier reserves outside the Polar region (Bolch et al., 2012; Azam et al., 2018, 2021). One of the significant glaciers among them is the Gangotri group glacier. Glacier melt

* Corresponding author.
E-mail addresses: praveen@iirs.gov.in (P.K. Thakur), a.stein@utwente.nl (A. Stein), vaibhav@iirs.gov.in (V. Garg), arpit@iirs.gov.in (A. Chouksey), prakash@nrsc.gov.in (P. Chauhan).

https://doi.org/10.1016/j.asr.2023.03.001
0273-1177/

runoff water contributes to major river systems like the Ganges, which significantly impacts the livelihood of millions of people (Jain, 2008). The upstream snowmelt runoff and the glacier dynamics influence river water availability (Kaser et al., 2010; Immerzeel et al., 2010, 2020; Wood et al., 2020; Huda et al., 2021; Orr et al., 2022). Velocity, elevation changes, and thickness are the key parameters driving glacier dynamics (Gantayat et al., 2014; Kumar et al., 2013; Thakur et al., 2016). The longest record of terminus retreat shows a significant variation in multi-decadal retreat and has been reported to reduce in the recent decade. A consistent mass loss, thinning of debris-cover tongues, and growth of supraglacial lake in recent years indicate the emerging need to understand the dynamics of the Gangotri glacier to anticipate the impact of future water resource constraints.

A comprehensive record of Gangotri glacier dynamics was missing due to its inaccessibility. For example, a glaciological and mass balance study has not been carried out at Gangotri. However, in some Himalayan glaciers, the in-situ mass change analysis is carried out up to 7 km (Azam, 2021). Further, the glacier dynamics can be extrapolated from the suspended sediment concentration from the proglacial stream (Kumar et al., 2018). On contrary to the in-situ observations, remote sensing can be used to estimate, map, and monitor glacier velocity, glacier extent, ice-elevation variations, crevasses, glacial lakes, glacier volume, and equilibrium line altitude, at a larger scale (Khalsa et al., 2004; Berthier et al., 2007; Mathieu et al., 2009; Wessels et al., 2002; Scherler et al., 2008; Karimi et al., 2012; Bhambri et al., 2012; Kumar et al., 2013; Thakur et al., 2017, 2018). The information from the satellite observation is crucial to understand the glacier mass balance, glacier lake monitoring, and river discharge due to the seasonal variation in snow cover and glacial ice (Kaser et al., 2010; Berthier et al., 2007; Huss et al., 2008; Chen and Ohmura, 1990; Singh et al., 2006). Therefore, remote sensing can be used as an alternative to understand the glacier dynamics of the Gangotri glacier (Kulkarni et al., 2007; Thakur et al., 2017).

Previous studies have utilized various remote sensing techniques to understand the glacier dynamics, combining in-situ observations with satellite velocity and snout retreat calculations (Bhambri et al., 2012). A rapid recession of snout is observed using the static Global Positioning System (GPS), kinematic GPS, and satellite survey (Kumar et al., 2009; Bhambri et al., 2012). The snout retreat indicates the overall velocity and health of the glacier, but it does not provide information about the spatial change in velocity (Gantayat et al., 2014; Leprince et al., 2007; Saraswat et al., 2013; Dehecq et al., 2019). The Gangotri glacier undergoes an average summer speed up to 92% higher-than-winter velocity change (Satyabala, 2016). However, multi-temporal remote sensing with a weekly or monthly temporal scale is required to quantify the changes more accurately due to the complexity of the feature or amplitude tracking method used for velocity mapping. Moreover, the dynamics involve the change in elevation of the glacier, which can be calculated from active remote sensing techniques like differential interferometry.

The glacier volume change is a major component in understanding glacier health, which is only somewhat possible with satellite information. The glacier ice volumes or ice thickness can be estimated using volume–area (V–A) relations (Chen and Ohmura, 1990; Bahr et al., 1997), slope-dependent ice-thickness estimations, (Haeberli and Hölzle, 1995) and spatially distributed ice-thickness models (Cuffey and Paterson, 2010; Huss and Farinotti, 2012; Li et al., 2011; Clarke et al., 2013; McNabb et al., 2012; Farinotti et al., 2009a,b). Further, glacier area and length records available from field surveys and remote sensing data have been used to create Power-law relationships for glacier volume/area, volume/length, and volume/area/length (Chen and Ohmura, 1990; Bahr et al., 1997; Linsbauer, et al., 2009). Therefore, combining seasonal variation in velocity and volume change can be a better proxy for understanding glacier dynamics.

The current study utilized multiple remote sensing data and in-situ observations to understand the Gangotri glacier dynamics. Here, we estimated (a) seasonal and annual glacier velocity using optical and Synthetic Aperture Radar (SAR) datasets, (b) summer season and long-term elevation changes using Interferometric SAR (InSAR)-based DEM data, (c) depth or thickness using various modelling techniques, and finally d) validated the snout depth with model-based outputs of Gangotri glacier. We used the multi-satellite remote sensing techniques to quantify the seasonal variation of velocity, including short- and long-term changes that have not been addressed in previous studies. We employed InSAR-based elevation changes at a shorter time scale to understand the elevation changes.

The present research work has been organized into four sub-sections. Section 2 provides a brief overview of the study area, instruments, datasets, velocity estimation using optical and SAR images, volume estimation, elevation change, and uncertainty analysis; Section 3 provides the main results, followed by a discussion; Section 4 is conclusion with information on a further scope.

2. Data and methods

2.1. Datasets

The current study area is Gangotri Glacier, located in Uttarakhand, India. The Gangotri glacier is the second largest in the Himalayan region, with 26 km in length and width varying between 0.2 and 2.5 km (Bisht et al., 2015). The elevation starts at 4 km and extends to 6 km (Bhambri et al., 2012; Thakur et al., 2016). The glacier's main trunk is oriented in North-West (NW) direction with a 29% lower ablation area covered with supra-glacier lake and debris (Bhambri et al., 2012). The Gangotri glacier has eight tributaries, with significant contributions coming from Kirti (11.05 km), Raktvarn (15.90 km), and Chatu-

rangi (22.45 km) glaciers. Mass movement, erosion, and deposition resulted in present landforms and glacial-periglacial features (Fig. 1b & c; Dhote et al., 2021).

We used multiple data sets to calculate the velocity and elevation changes (Huber et al., 2009; Fritz et al., 2011; Krieger et al., 2007). The elevation change is obtained from TanDEM-X (TDX) and TerraSAR-X (TSX) interferometric data sets. The velocity map is derived from Sentinel-1 (December 2016–January 2017), Sentinel-2 (September 2018–September 2019), and Advanced Land Observing Satellite - Phased Array L-band Synthetic Aperture Radar (ALOS-PALSAR)-2 Polarimetric SAR data (March–April 2015). More details on the datasets can be found in Tables 1 and 2. In-situ observations during October 2012 and September 2014 from the "Differential Global Positioning System" (DGPS) were used to evaluate velocity, elevation change, and snow ice thickness. Further, Terrestrial Laser Scanner (TLS) was also used to measure snout position, profile, and height during October 2014 (Fig. 1b). Here, we considered multispectral images for mid and late ablation season as compared to SAR images to avoid seasonal impact (Table 1). The Shuttle Radar Topography Mission (SRTM) Digital Elevation Model (DEM) was used to derive the slope and aspect of the glacier to understand its dynamical properties of the glacier. SRTM has a vertical accuracy of ±16 m compared to the Advanced Spaceborne Thermal Emission and Reflection Radiometer (ASTER) DEM (Racoviteanu et al., 2007; ASTER GDEM Validation Team, 2011; Rodríguez et al., 2006). Moreover, we used SRTM DEM to remove flat earth and topographical phase unwrapping (Joughin et al., 2010) in the interferometric SAR processing step. More details on phase unwrapping can be found in the following section. Finally, we used Defense Geoinformatics Research Establishment (DGRE) Automatic Weather Station (AWS) observation of air temperature near Gangotri glacier to infer dynamic properties at various processing levels.

2.2. Estimation of glacier velocity using InSAR and elevation change using DInSAR approach

We estimated the Gangotri glacier velocity using SAR interferometry. Sequential interferometric pairs of the pre- and post- events were required to estimate the changes. Moreover, SAR interferometric techniques can be used to derive glacier velocity at centimeters level accuracy (Bhattacharya et al., 2012). The interferogram can be used to detect the ground movement from the small phase shift between the pre- and post- event dataset. However, the presence of phase shift can be majorly due to the ground's

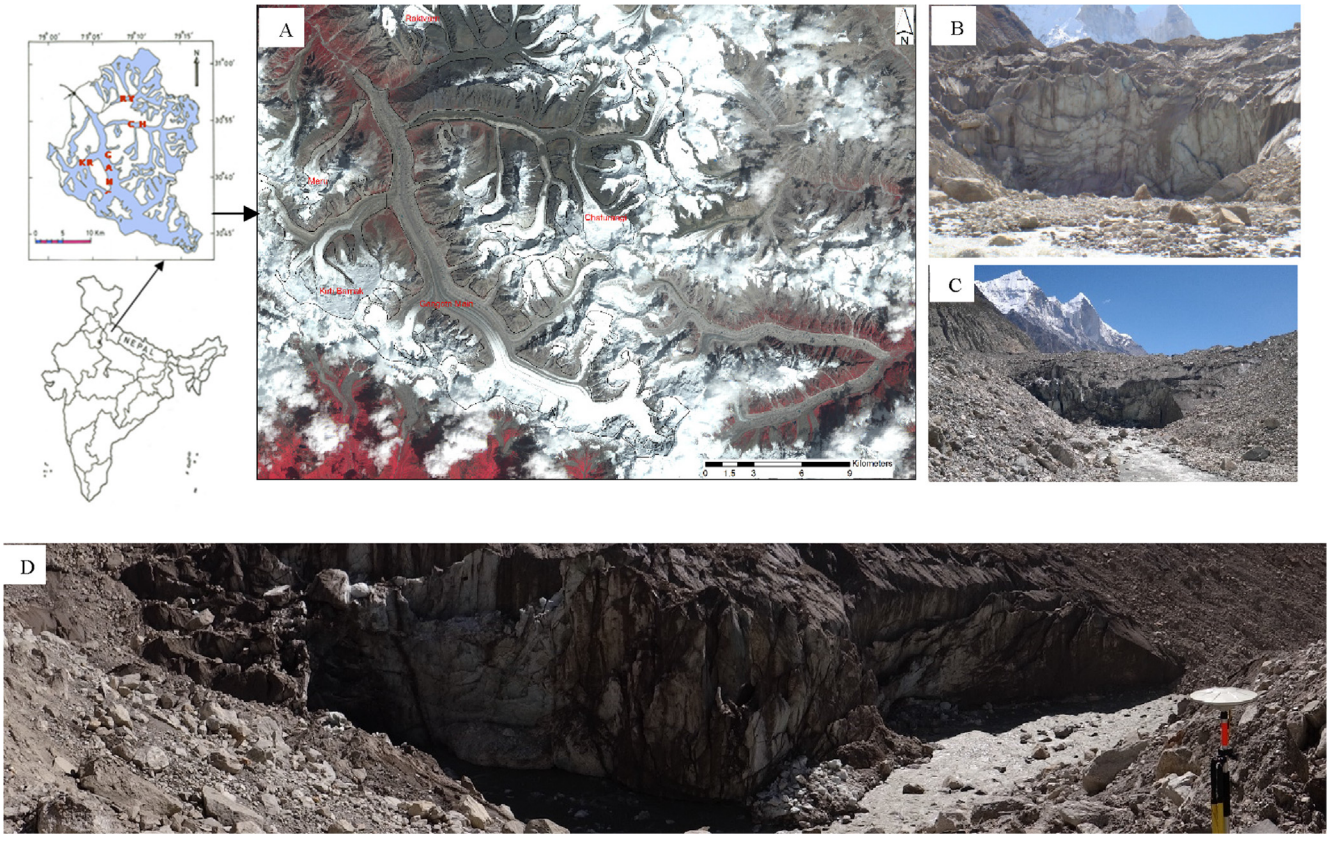

Fig. 1. Study area description (Gangotri glacier). (a) False Color Composite (FCC) image of Gangotri Group of Glacier as seen in Indian Remote Sensing (IRS) Linear Imaging Self-Scanning Sensor (LISS-IV) image of 20 Sep 2012, and glacier outline of 1960s is overlaid over the glacier, (b) frontal view of Gangotri glacier snout during September 2008, (c) same as (b) but for September 2014, and d) same as (c) but panorama view. The location of DGPS is on the right bank of glacier snout.

Table 1
SAR data used for the Gangotri glacier to measure glacier velocity (ERS, TANDEM-x, PALSAR-2) and elevation (Tandem-x) changes with results.

Satellite	Acquisition Mode	Band and acquisition Path	Date days	Period	Normal Base Line m	Displacement cm day^{-1}		Error cm day-1			
						Azimuth	Range	Azimuth	Std. Dev.	Range	Std. Dev.
ERS 1	Monostatic	C - ascending	25/03/1996	T1	75.34						
ERS 2	Monostatic	C - ascending	26/03/1996		75.34		9.00			1.74	
ERS 1	Monostatic	C - descending	11/04/1996	T2	104.3						
ERS 2	Monostatic	C - descending	12/04/1996		104.3		14.00				
TanDEM-X	Bistatic	X - ascending	*09/06/2012*	T3	248.62						
TanDEM-X	Bistatic	X - ascending	*01/07/2012*	T4	241.55	04.50	02.50	1.04	0.8	0.59	0.50
TanDEM-X	Bistatic	X - ascending	*23/07/2012*	T5	228.93	02.70	01.50	1.05	0.60	0.47	0.40
TanDEM-X	Bistatic	X - ascending	*05/09/2012*		209.98	01.90	00.98	1.09	0.6	0.10	0.13
PALSAR-2	PolInSAR	L-band	*22/03/2015*	T6	87.43		NA				
PALSAR-2	PolInSAR	L-band	*19/04/2015*								
Sentinel-1	Dual Pol	C-band descending	*22/12/2016*	T7			10.2			0.63	
			28/12/2016								

Table 2
Optical image pairs used for glacier velocity estimation using feature tracking approach with results.

Satellite*	Date Pair	Window Size		Resolution (m)	SNR	Time	Mean Velocity	Mean Velocity
		Initial	Final			(m/day)	(m/day)	(m/year)
Landsat 5/7	9Sep98–22Oct99	64	32	30	0.9	408	0.060	21.72
Landsat 7	8Oct00–20Oct01	64	32	15	0.9	377	0.052	19.09
Landsat 7	22Oct99–8Oct00	64	32	15	0.9	352	0.067	24.62
Landsat 7	20Oct01–8Jun02	64	32	15	0.9	231	0.073	26.46
Landsat 7	22Oct99–20Oct01	128	64	15	0.9	729	0.053	19.33
Landsat 5/7	9Sep98–8Oct00	128	64	30	0.9	760	0.046	16.94
Landsat 8	18Sep13–21Sep14	64	32	15	0.9	369	0.051	18.51
Sentinel-2	19Sep18–19	128	32	10	0.9	365	0.043	15.31
IRS-1C/D	22Oct00–08Jul02	256	64	5	0.9	624	0.032	11.75
IRS-1C/D	22Oct00–05Oct03	256	64	5	0.9	1078	0.021	11.28
IRS-1C/D	8Jul02–20Oct05	256	64	5	0.9	1200	0.029	10.51
IRS-1C/D	8Jul02–5Oct03	128	32	5	0.9	454	0.047	17.23
IRS-1C/D	5Oct03–20Oct05	256	64	5	0.9	746	0.021	11.39

* In both Landsat and IRS datasets, PAN data was used for feature tracking, band 4 was used for Landsat-5.

horizontal or vertical component. The horizontal shift is obtained by separating the topographic component from a non-zero baseline. Further, we used DInSAR to generate the elevation for each time. DInSAR data processing involves image co-registration, baseline estimation, interferogram and coherence generation, flat earth and topographical phase removal, and phase unwrapping to obtain elevation (Just & Balmer, 1994; Hanssen, 2001). Since the TanDEM-X data have high coherence, we expect the minimal influence of phase unwrapping for the derived elevation (Rizzoli et al., 2017).

The complete phase information is crucial for calculating displacement and elevation changes (Wegmüller & Werner, 1997; Schneevoigt et al., 2012). The unwrapped phase is transformed to velocity values considering certain assumptions as (a) glacier flows parallel to the surface topography, (b) DEM provides terrain surface topography of a glacier, (c) surface elevation changes between two SAR image acquisitions are negligible, and (d) the atmospheric effect is negligible (Li et al., 2008).

Next, we used bi-static images from TanDEM-X data to calculate the elevation changes over the Gangotri glacier. In general, stereo pairs can be used to generate a DEM from a reference tie point method. However, in InSAR processing, the unwrapped phase, with the help of reference SRTM data, is used to create a high-resolution DEM. The actual height is obtained by fitting a polynomial function between phase and height (Bhattacharya et al., 2012; Small et al., 1993; Costantini, 1998).

$$h = \sum_{i=1}^{M} c_i \varphi_e^{i-1} \tag{1}$$

where $c_i, i = 1, \cdots, M$, are the coefficients, φ_e^{i-1} is unwrapped phase value of i^{th} pixel, M is the total number of coefficients and h is the actual height. Further, a co-registration was also performed with the TanDEM-X data to obtain elevation data, seasonally following the method given in Nuth and Kääb (2011). Finally, the elevation change is calculated from the difference between each period (Table 1).

2.3. Glacier surface velocity estimation using feature tracking approach

The loss of coherence between images significantly challenges the SAR interferometric technique for velocity estimation. The loss of coherence can be due to meteorological conditions, movement, snowfall, and larger temporal resolution between images (Joughin et al., 2010). Loss of coherence can lead to less cross-correlation between the images, which leads to enormous glacier velocity values. To avoid such a situation, we employed feature-tracking techniques to determine the glacier velocity (Scherler et al., 2008; Leprince et al., 2007; Joughin et al., 2010). In multiple temporal images, search windows of user-defined pixels are used to identify features like a crevasse, supra glacier lakes, and big debris rock. First, the single-look complex is converted into a multi-look to make the data set uniform and reduce speckle noise. Following, both SAR images are used to calculate the sub-pixel correlation. Similarly, a pair of multi date *ortho*-rectified optical images were used for calculation of sub-pixel correlation. Feature tracking identifies similar features on two temporal data sets for velocity estimation (Huss et al., 2008; Paul and Linsbauer, 2012). The shift in features between the images is the criteria for estimating the velocity. Here, we used the ENVI module COSI-Corr package (https://www.tectonics.caltech.edu/) to compute the glacier velocity. Cosi-Corr uses a feature tracking method to identify similar objects between two images iteratively to find the best possible correlation. A detailed description of the algorithm can be found in Leprince et al., (2007). The parameters used to obtain the velocity map are given in Table 2. We avoid pixels having signal-to-noise ratio (SNR) < 0.9 and glacier movement greater than 85 m. The velocity field can be estimated using the difference in the acquisition time between the two images.

$$D_{h=}\sqrt{(R_x u)^2 + (R_y v)^2} \tag{2}$$

where D_h is the translation movement; R_x and R_y are the spacing between pixels in the x and y directions, respectively; and u and v are the offsets in East-West and North-South directions. Further, local averaging is carried out to filter out pixels showing very high glacier velocity values, which are termed noise (Bisht et al., 2015) due to image correlation uncertainties over snow-covered pixels. Annual glacier velocity (m/year) has been calculated by dividing the net movement value (m) by the time interval in days between the two images and multiplying by the number of days in a year.

2.4. Estimation of glacier volume

We used a slope-dependent and surface velocity method to estimate the ice thickness along the Gangotri glacier (Gantayat et al., 2014; Frey et al., 2014; Cuffey and Paterson, 2010; Farinotti et al., 2009a,b). The obtained glacier volume from multi-sensor data is validated against TLS at the glacier snout. We used TLS observation from the 15–17 September 2014 data for the validation.

2.4.1. Volume – Area (V-A) scaling relationships

V–A scaling method is widely used for ice volume estimations (Bisht et al., 2015; Bahr et al., 1997; Huss and Farinotti 2012). Ice volume is calculated as a function of its surface area for large glaciers due to their high thickness. Area-related scaling techniques are relatively more straightforward and faster in the application, hence extensively applied. Area data were being measured and compiled long before digital terrain information became available, hence, long-term data is available (Bahr et al., 1997). V–A scaling relation is generally represented as (Frey et al., 2014; Bisht et al., 2015):

$$V = cA^{\gamma} \tag{3}$$

where V shows the glacier volume, A is the glacier area, and γ & c are two scaling parameters. To validate the results from other ice thickness methods and measurements, Eq. (3) can be converted into the thickness–area relation as (Frey et al., 2014; Bisht et al., 2015):

$$H = cA^{\beta} \tag{4}$$

where H is the ice thickness and $\beta = \gamma - 1$. We combined scaling from Bisht et al. (2015) and Frey et al. (2014). The scaling parameters used in the study are given in the Table 3.

2.4.2. Slope-dependent ice-thickness estimation

Here we followed Haeberli and Hölzle (1995) method to estimate glacier volume using average surface slope and vertical glacier relief. We obtained the parametrization for estimating the ice depth and volume from Frey et al. (2014) for the Himalayan-Karakoram (HK) glaciers. Following the GlabTop-2 and slope-dependent method given by Frey et al., (2014), we estimated ice-thickness over the Gangotri glacier. The slope-dependent method is computationally efficient, but at the same time, fewer inputs result in under- or over- estimation of ice thickness. The main parameters used in this model are given in the Table 4.

Paul and Linsbauer (2012) used a hybrid approach using inputs from Clarke et al. (2009) and Li et al. (2011), which considers the flow dynamics and enables the bed estimation (Bisht et al., 2015). The GlabTop model approach digitizes flow-lines and accounts for basal shear stress (τ) at every 500 m interval. The slope dependent model does not consider variable 'τ' but uses mean value (Bisht et al., 2015).

Table 3
Parameter of the applied V-A relations.

Source	C	γ
Chen and Ohmura (1990)	0.2055	1.36
Bahr et al. (1997)	0.191	1.375
LIGG et al., (1988)	0.8433	1.3

Table 4
Slope Dependent Model Parameters with GlabTop Results.

Name of glacier branch	Length (km)	ΔH (km)	α(rad)	τ	Ice depth (m)	Area Covered (km^2)
Gangotri main	30	3.2	0.10626	150	200.42	68.4
Raktvarn	10.27	2	0.19233	150	111.21	47.88
Chaturangi	15.18	1.2	0.07888	129.62	233.10	64.89
Swachand	6.81	1.15	0.16729	126.7413	107.87	16.11
Malandi	4.26	0.85	0.19694	104.9013	75.97	4.58
Meru	8.53	1.45	0.16837	140.7513	119.03	5.57
Kirti	9.01	2	0.21843	150	98.10	31.60
Ghanohim	4.03	0.6	0.14779	80.72	77.68	11.83
Gangotri2	4.7	1	0.20963	116.8	79.54	19.47

The DEM used in the study is converted into 50 m contour lines. Further, a slope map is obtained to calculate the 'τ' (Bisht et al., 2015). The estimated slope map and 'τ' were used as inputs for the ice thickness distribution along the glacier flow lines. We used the interpolation method (TopToRaster function – ArcGIS) to obtain ice thickness over the entire glacier (Bisht et al., 2015).

2.4.3. Ice thickness retrieval from velocity measurement

We obtained the ice thickness value following the velocity estimation given in Section 2.3. The thickness is obtained from the relationship between basal shear stress and glacier velocities (Glen, 1955; Cuffey and Paterson, 2010). The model assumes the glacier is a parallel-sided slab of ice with thickness H on a rough plane of slope α. The sliding of the slab is considered negligible here, and the thickness is much less than its length and width (Bisht et al., 2015). The slab is perpendicular to the plane with a unit cross-section. The slab's weight is ρgH, where ρ is the density of ice, g is the acceleration due to gravity, and H is the height of the slab (Cuffey and Paterson, 2010; Bisht et al., 2015). The glacier ice thickness from a given glacier velocity pair and slope (Cuffey and Paterson, 2010) can be obtained using

$$H = \sqrt[n+1]{\frac{(n+1)\cdot(u_s - u_b)}{2A\cdot(f\cdot\rho\cdot g\cdot sin\alpha)^n}} \quad (5)$$

where u_s is surface glacier velocity derived as described in Section 2.3 and u_b is basal glacier velocity, f is a scale factor, i.e., the ratio between the driving stress and basal stress along a glacier, ρ is the ice density, A is a creep parameter depending upon temperature, fabric, grain size and impurity content, g is acceleration due to gravity (9.8 m/s^2) and α is the slope. Considering the Gangotri glacier a temperate region, we used $f = 0.8$ (Frey et al., 2014; Li et al., 2011). We assigned a constant value of 900 kg/m^3 to ρ (Cuffey and Paterson, 2010), A has a value of 3.24 × 10^{-24} Pa^{-3} s^{-1} for temperate glaciers (Cuffey and Paterson, 2010), and the slope is estimated from 90 m SRTM DEM.

2.4.4. Ground based measurement of ice thickness and uncertainty estimation

We used a Differential Global Positioning Sensor (DGPS) and TLS to collect the field measurement of ice thickness at the Gangotri glacier snout during September 2014. First, TLS and its reflectors were kept 30–100 m apart. DGPS measured the position of TLS and its reflectors. TLS used for the first time to measure the ice thickness of the Gangotri glacier. TLS data was also used to measure the depth of snout ice. Further, the TLS-based scan of the Gangotri snout was overlaid over the modeled ice thickness outputs. The DGPS measurements were used to validate the TanDEM-X DEM elevation for 2012. For the year 2014, both DGPS and TLS positioning were used to validate the elevation at the snout.

Further uncertainty in the glacier ice estimation is carried out following various literatures. The uncertainty in the scaling factor was set at 0.1, as Gantayat et al. (2014) suggested. We used a creep factor of 8.24 × 10^{-25} (Farinotti et al., 2009a,b) and an ice density of 90 kg/m^3 i.e., 10% of the Gangotri glacier density. We obtained a slope uncertainty of 0.001 from the SRTM 90 m DEM (Table 5).

3. Result and discussion

3.1. Velocity (InSAR) and elevation change (DInSAR) from SAR dataset

We defined sequential time labels for various datasets (e.g., T1, T2 …T7) to estimate the velocity and elevation change (Table 1). The interferometric fringe shows a consistent pattern of horizontal velocity towards the flow direction of Gangotri and its tributary glaciers (Fig. 4a).

Table 5
Error estimation for optical image based feature tracking based glacier velocity.

Satellite	Band Resolution (m)	SNR	SNR achieved	Accuracy (m)	Error	Error in velocity (cm/day)
Landsat	15	0.9	0.99	14.85	0.15	0.04109
IRS	5	0.9	0.89	4.45	0.55	0.15068

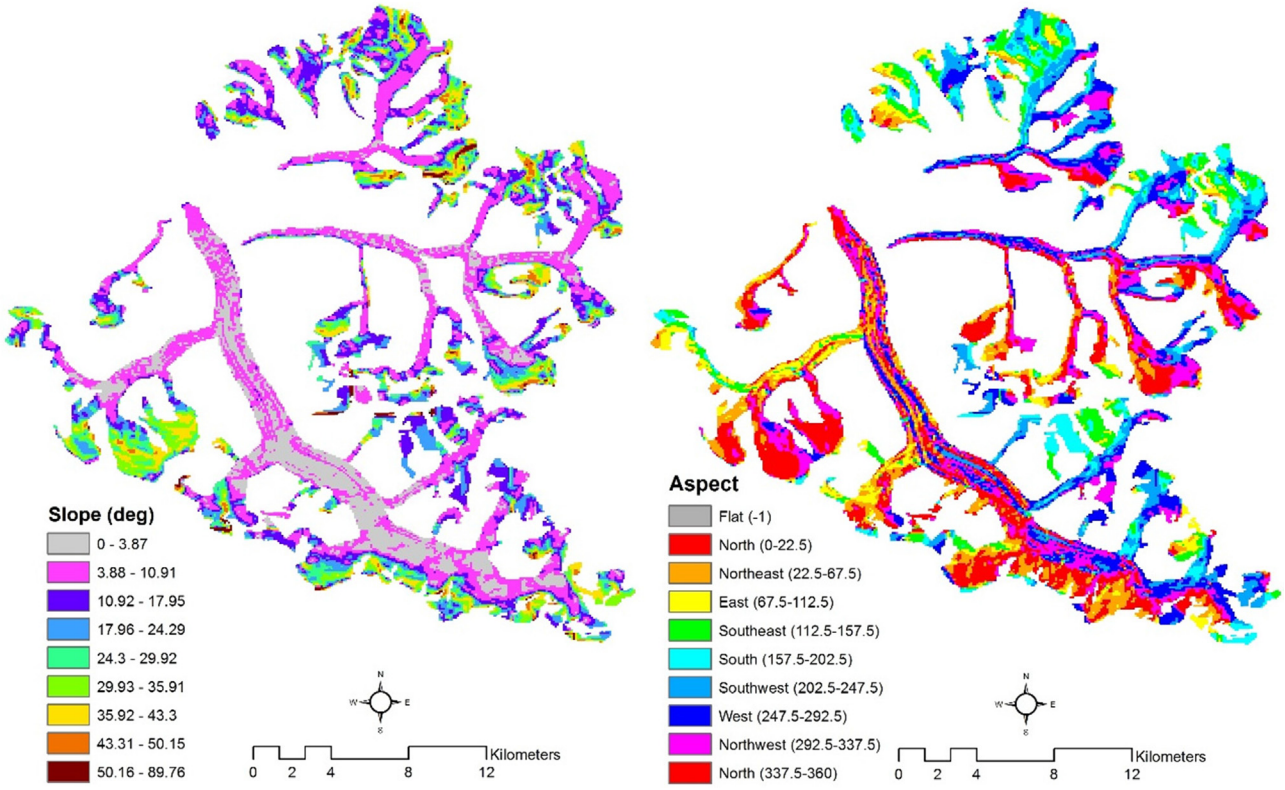

Fig. 2. Gangotri glacier slope and aspect maps obtained from Shuttle Radar Topography Mission (SRTM) Digital Elevation Model (DEM). Here we used 90 m DEM for the slope and aspect.

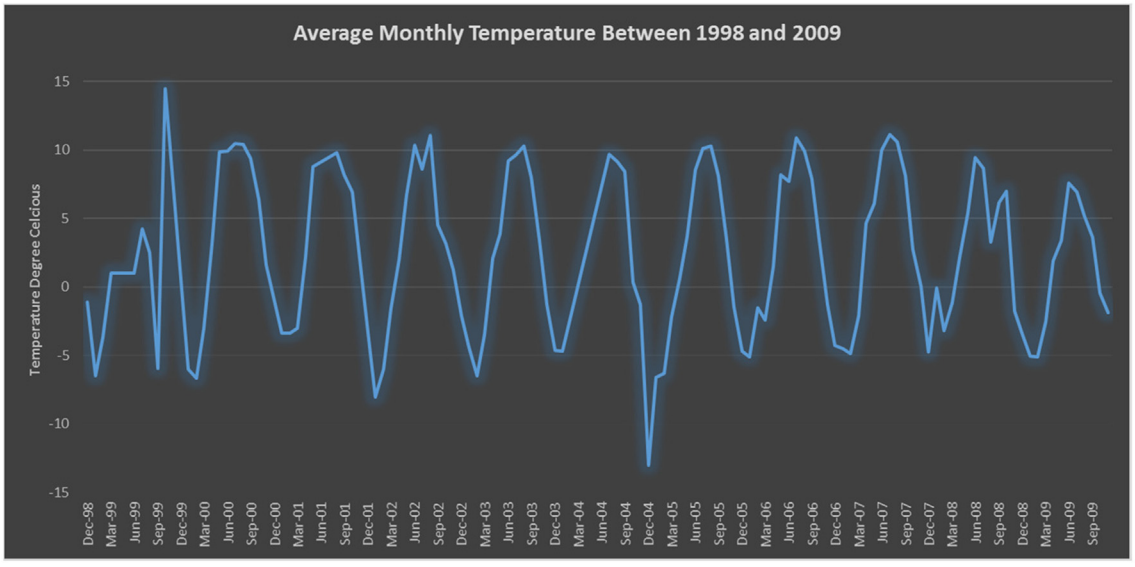

Fig. 3. Mean monthly temperature at Gangotri snout area obtained from Defense Geoinformatics Research Establishment (DGRE) Automatic Weather Station (AWS) for the 1998–2009 period.

A coherence of 0.37 in ERS data set and 0.67 (average) for the TanDEM-X signifies a reliable output of velocity and elevation (Wangensteen et al., 2005). The low mean coherence for ERS is majorly due to seasonal snowfall, wet snow, and snowmelt (Strozzi et al., 1999; Negi et al., 2012). We observed a 9 cm/day and 14 cm/day velocity along the range direction for the T1 and T2 periods (Fig. 4b). However, careful consideration is required not to convert these results into an annual time scale due to the variation in velocity during different seasons.

A high glacier velocity is observed along the Southwest, West, Northwest, and North aspects of Gangotri glacier

(Fig. 4b). This can be due to the presence of these aspects on a steep slope (Fig. 2). Moreover, movement in such areas is gradually increasing with slope, and this movement is linearly correlated with 99% of slope area. A slope above 50° (∼one percent of the glacier) is not considered for this analysis to avoid the uncertainty from free fall of snow. The velocity rate in the Northwest and North aspects was as high as compared with that of the Southeast during early summer. A few areas in the Southwest, Northwest and South aspects also show high-velocity rates. Most of these aspects fall under the low, moderate, and high slope regions (slope 30–50°) shown in Fig. 2. However, lack of coherence due to the presence of snow or snowmelt/snow freeze between two dates can result in above or below normal velocity rates (Fig. 4d & e). High coherence is observed for Sentinel-1A/1B SAR pairs along the line of sight (Fig. 4e).

Next, we estimated the elevation changes from the TanDEM-X data sets. An interferometric coherence of 0.8 is observed majorly due to concurrent observation from the TanDEM-X pairs. The high correlation neglect variation in phase jumps, whereas the low correlation attributes to volume decorrelation (Kumar et al., 2013). The DEM generated for low correlation areas introduces phase unwrapping errors, leading to enormous elevation estimation values. Therefore, we used a coherence area above 0.4 for DEM calculations. A DEM was generated for 9th June, 1st July, 23rd July, and 5th September 2012 (Fig. 5a). Further, the elevation change is calculated from differences between a 1st day DEM, a DEM at the 22nd day and a DEM at the 44th day (Fig. 5b). The TanDEM-X DEM can provide an absolute vertical accuracy up to 10 m and a relative height error equal to 1.77 m (Huber et al., 2009; Gruber et al., 2009; Detlev

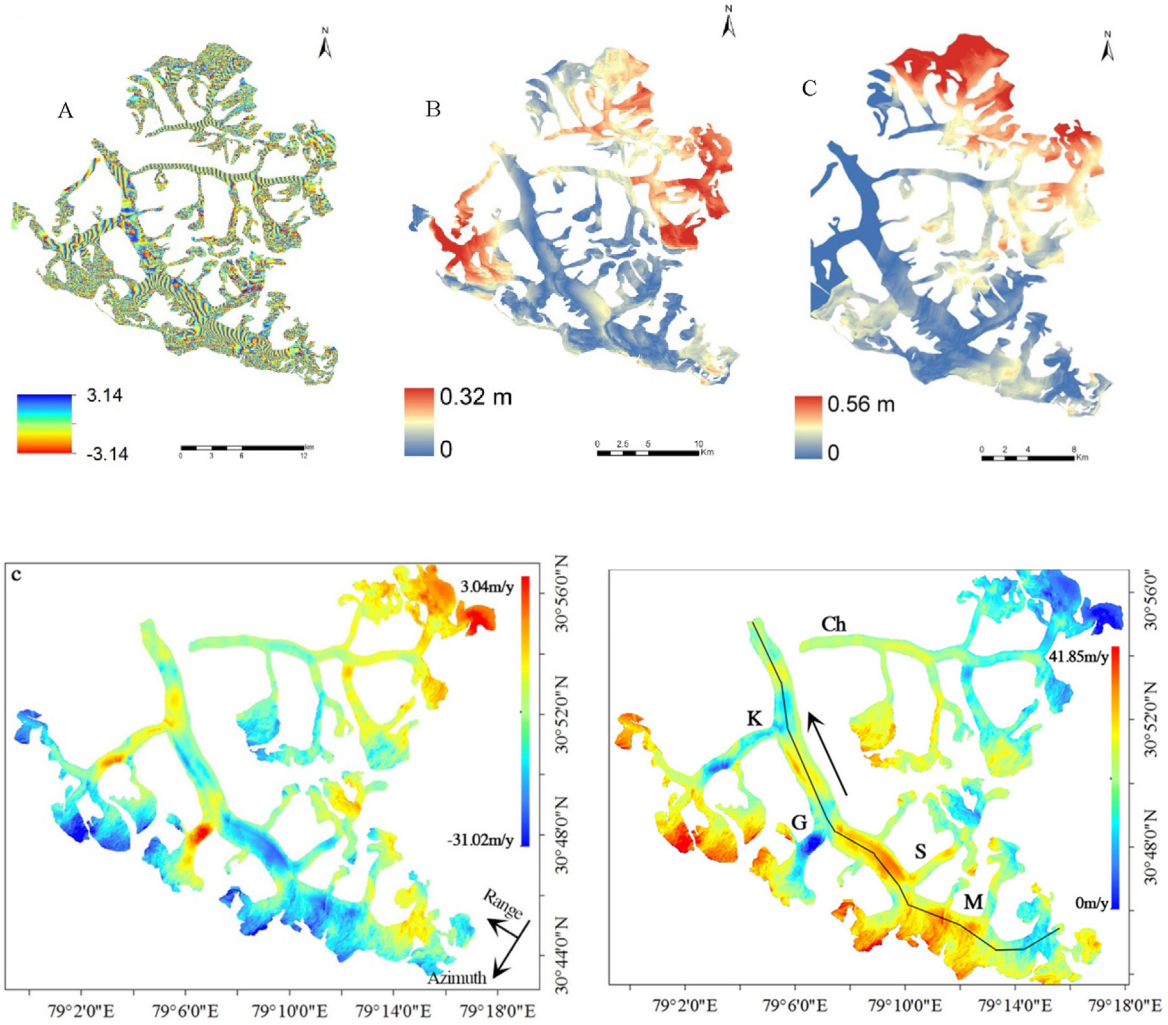

Fig. 4. Glacier velocity from Differential Interferometric Synthetic Aperture Radar (DInSAR) (a) ERS interferogram, (b) glacier velocity for 25–26 March 1996, (c) same as (b) but for 11–12 April 1996, (d) Sentinel-1A/1B DInSAR based glacier velocity results in Line of Sight (LoS), and (e) Sentinel-1A/1B DInSAR based glacier surface velocity (22–28 December 2016). The text in (e) refers to various branches of Gangotri glacier, i.e., Ch represents Chaturangi glacier, K represents Kirti Glacier, G represents Ghanohim branch, S represents Swachhand branch and, M represents Mainadi glacier branch.

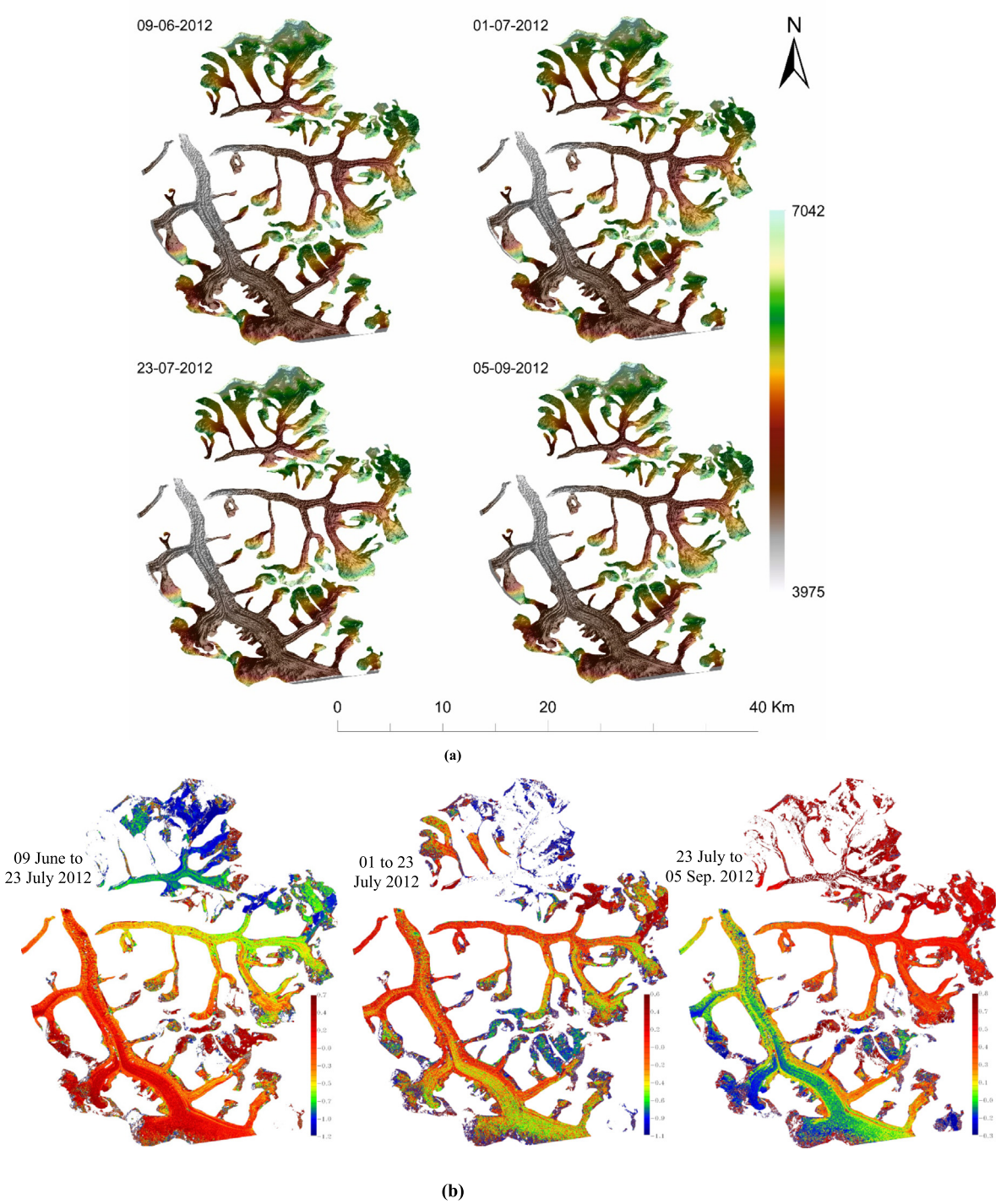

Fig. 5. Glacier elevation change. (a) TanDEM-X based DEM for different periods of 2012 for Gangotri glacier, (b) TanDEM-X based elevation difference maps for main Gangotri and its tributary glaciers, (c) elevation difference between STRM and TANDEM-X (30 m) for Gangotri group of Glaciers, and (d) elevation (co-registered) difference histogram for Gangotri glaciers.

et al., 2010). The variation in elevation observed in TanDEM-X is majorly from relative height measurement using a DGPS and local topography (Wells et al., 1999; NRC, 1995).

We observed a mean elevation change of −0.12 m (range −1.12 to 0.7 m) during the T3 (Fig. 5b) period. In October 2012, six to nine DGPS points were taken near the snout (on glacier ice and ice-free area below snout) of the glacier. TanDEM-x DEM of T3 time was validated with these limited points with root mean square error (RMSE) of 8.3 to 11.32 m, which is similar to 10 m relative height error reported by Detlev et al. (2010) and Pandit et al., (2014). However, the mean values of −0.042 m (range −1.06 to 0.58 m) and 0.09 m (range −0.32 to 0.83 m) were observed

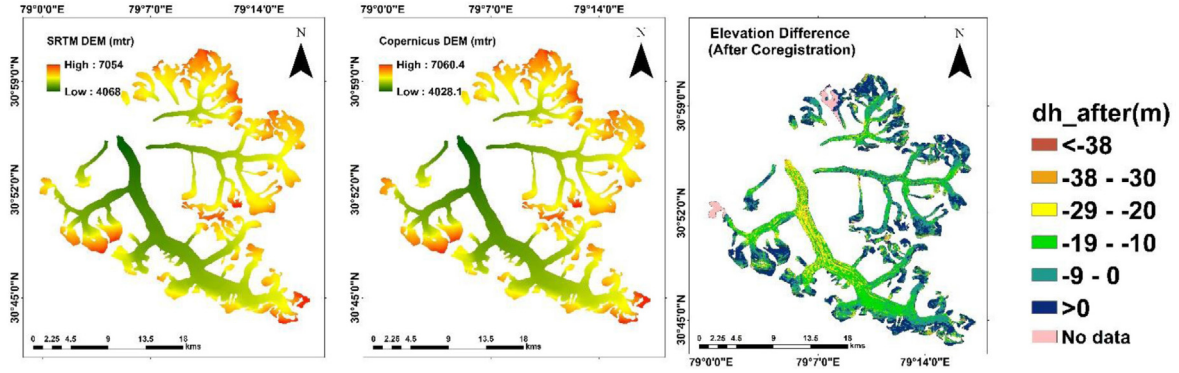

(c)

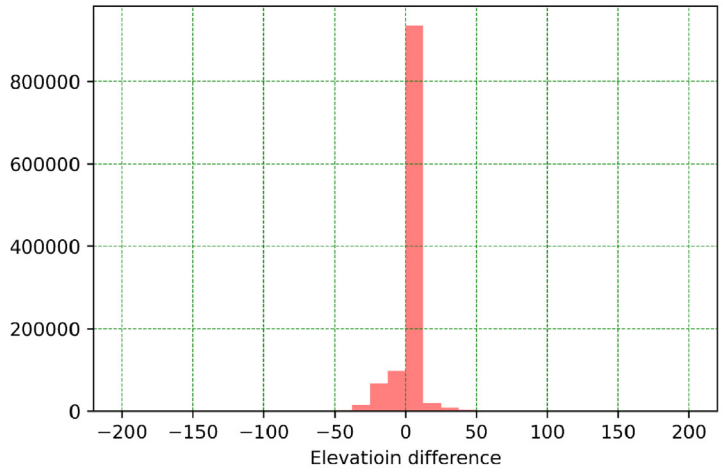

(d)

Fig 5. *(continued)*

for the T4 and T5 periods respectively. Further, we observed that in mid-summer, there is a net decrease in elevation as compared to a slight increase during the summer or end of the ablation season (period T3 and T4). The change in the ablation period may be due to the high melting rate of snow and ice during June to August compared to less rate during the end of the ablation season because of possible snowfall. Pandey et al. (2016) reported a net mass balance of −0.4 m/year for the 2011–2013 period. An annual average loss of −0.38 ± 0.65 m of ice was observed between 2000 and 2014. Here we also used the difference between TanDEM-X and SRTM DEM to calculate the mean elevation change. Moreover, the average elevation is within the range as previously reported (Pandey et al., 2016; Bandyopadhyay et al., 2019). The variation in elevation can be due to the seasonal effect. The long-term elevation change shows the ablation zone is experiencing thinning and gain is majorly over the accumulation zone (Fig. 5c & d). A mean elevation of −5.27 ± 9.1 m is observed during the 2000–2014 period.

Finally, the magnitude of error contributing to glacier velocity is evaluated for the Gangotri glacier. A non-moving area was initially defined to identify the error calculation towards the velocity. Here, we identified a mean velocity error of 0.53 cm/day (standard deviation ± 0.67 c m/day) for the azimuth direction. However, for the range direction, the velocity error is 0.02 cm/day (standard deviation ± 0.34 cm/day). The range error indicates that the azimuth direction velocity is more dominated by glacier velocity error. For the Gangotri glacier, the range velocity estimation is more reliable for active remote sensing [Table 1; Strozzi et al., 2002, 2006].

3.2. Glacier surface velocity estimation from optical datasets

We used medium to high-resolution information from LANDSAT, Sentinel-2, and IRS satellite images to estimate the velocity change for the 1998–2019 period (Table 2). The glacier velocity is derived using the feature-tracking method in the COSI-Corr software. We observed an average velocity of 17.4 m/year along the line of sight (Fig. 4e – along the black line) between 1998 and 2014 (Fig. 6a–d). For the upper glacier areas, the velocity accelerates from 24.0 to 58.5 m/year. Similar results are reported for the Gangotri glacier for a certain period (Gantayat et al., 2014). In addition, the snout retreat from

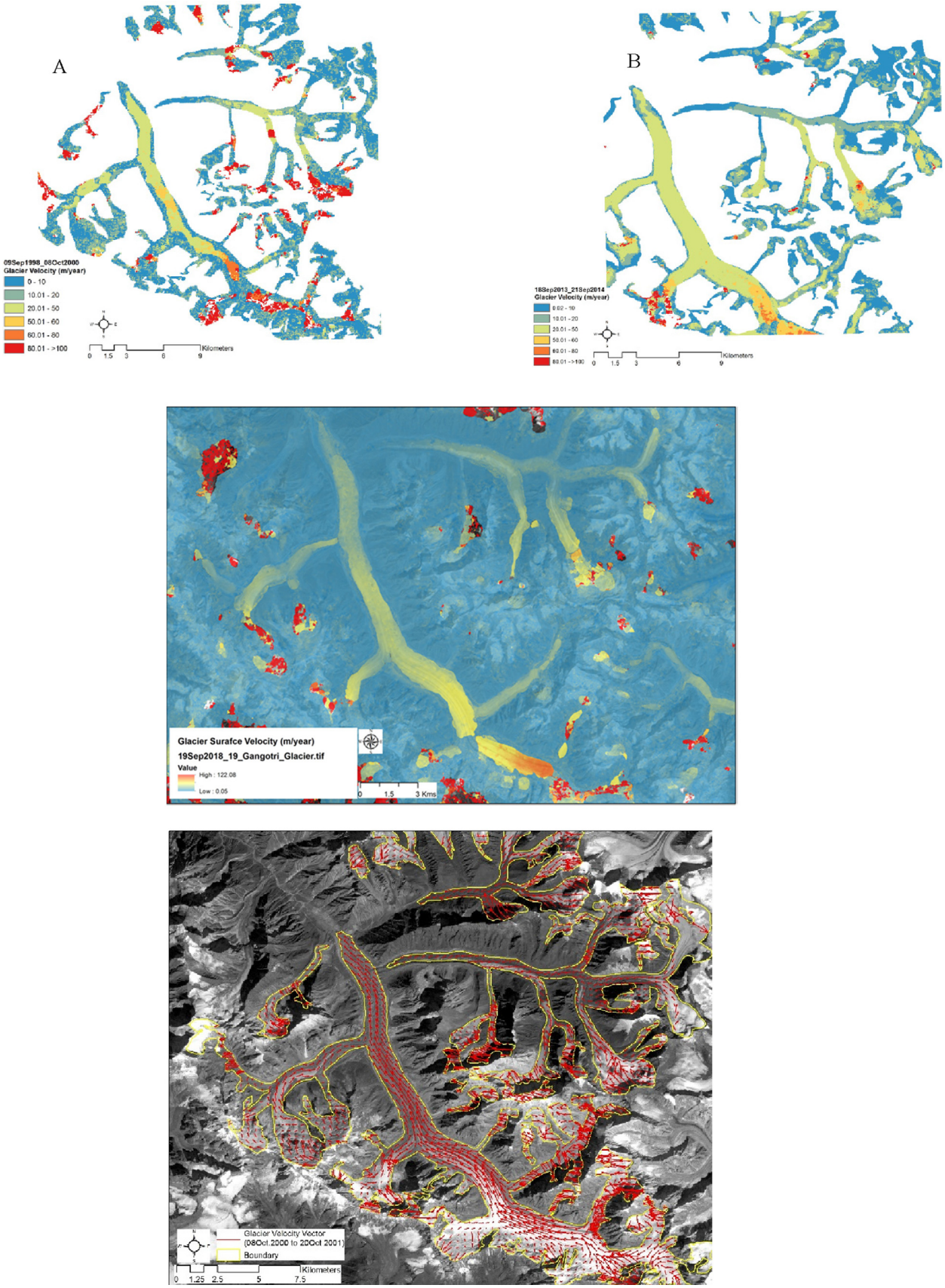

Fig. 6. Long-term surface velocity estimation from optical dataset. (a) Landsat feature tracking-based glacier velocity between 09/09/1998 and 08/10/2000, (b) same as (a) but for 18/09/2013–21/09/2014 period, (c) same as (a) but for Sentinel-2 19/11/2018–19/09/2019 period, and (d) shows the velocity vectors over Gangotri group of glaciers.

5.9 to 42 m/year, have been observed for the 1962–2006 period (Bhambri et al., 2012). However, the feature-tracking based method also noted an approximately 14–85 m/year of velocity in the accumulation region to 20–30 m/year near the snout for the 2004–2010 period (Gantayat et al., 2014). The earlier reported rapid static and kinematic GPS survey also finds a retreat of 12.0–13.7 m/year and 21.3 ± 3 m/year during 2004–2010 (Kumar et al., 2008; Saraswat et al., 2013). We observed a velocity from 2 to 30 m/year over the lower snout and ablation area. The higher altitude Gangotri glacier velocity ranges between 15 and 85 m/year, which is majorly for the clean ice area. Further, the average velocity in the north (lower; 28.1 ± 2.3 m/year) is significantly lower than in the southern (higher) regions (48.1 ± 2.3 m/year). The difference in velocity from previous studies is due to the mean value over glacier extent, different time scales, and spatial resolution. We observed a mean 0–0.351 m velocity uncertainty from IRS 1C/1D.

We observed that glacier velocity variation depends on the seasonal and annual time scales. The various studies on the Gangotri glacier also indicate a similar trend (Scherler et al., 2008; Bindschadler et al., 1977; Gudmundsson et al., 2000; Anderson, 2004; Satyabala, 2016). The seasonal variation in velocity change has commonly been attributed to snow or glacier meltwater at the bases of ice streams (Willis, 1995; Fountain and Walder, 1998; Joel et al., 2007; Satyabala, 2016). The mean velocity observed in 2012 could indicate a decreasing trend. Whereas, within each month, a unique velocity value for slope and aspect was observed. As shown in Table 1, the velocity during 2012 is greater between June and July than between July and September. This may be due to a decrease in surface melting, leading to a drop in sub-surface water pressure and resulting in a decreased sliding velocity in late summer (Anderson and Mackintosh, 2006). The presence of meltwater and basal melt result from velocity variation along the Gangotri glacier in early and late summer (Fountain and Walder, 1998; Satyabala, 2016). We observed a similar pattern during the springtime (Fig. 4e). Furthermore, during early summer, the temperature variation modulates the velocity. A maximum temperature of 10–12 °C during the June-July period was observed from DGRE's AWS (Fig. 3). Moreover, 30.7 m/year was also reported in early studies during the early summer (Negi et al., 2012; Singh et al., 2006, 2007; Satyabala, 2016). Therefore, our findings for the Gangotri glacier are more within the range of early reported velocity changes.

The DInSAR and optical estimated glacier velocity show lower values for ablation zones (0–20 m/year), whereas it is higher for the middle and upper ablation, and accumulation zones. We observed a significant (19–33%) reduction in velocity over the lower ablation zone during the 1998–2000, 20013–2014, and 2018–2019 periods. Previous studies also reported a similar trend (Bhushan et al., 2017; Dehecq et al., 2019). DInSAR finds a higher velocity for upper ablation, snout, and accumulation zones during the 2013–2014 and 2016–2017 periods. A low value in the optical data signifies the presence of snow, and large debris in optical images leads to low correlation. An enormous bias can also be identified in the SAR images due to the presence of spring snowfall. DInSAR and optical data have different advantages in monitoring glacier velocity and elevation change. For instance, the DInSAR can be used in all-weather conditions; and with various wavelengths, the glacier properties, like velocity, can be easily monitored. Therefore, optical images, DInSAR, and In-situ observations were required to understand the seasonal and annual variations in glacier velocity.

3.3. Glacier ice thickness estimation

We obtained glacier thickness from slope dependent and GlabTop2 methods. Both methods calculate the thickness based on the slope. However, the GlabTop produces thickness for height intervals (Paul and Linsbauer, 2012). Therefore, branch lines are digitized more intensely within the hydrological structure (Bisht et al., 2015). Here, basal shear stress (τ) is calculated for 500 m height intervals. We observed a large ice thickness from GlabTop and slope-dependent methods (Table 4) for the Gangotri main glacier (Fig. 7a & b). The tributary Chaturangi glacier also has a similar thickness as the Gangotri glacier; both glaciers exhibited the highest thickness values of 222.10 m (Gangotri) and 233.10 m (Chaturangi). The largest thickness along these glaciers signifies that the thickness is directly proportional to the area (Bisht et al., 2015). The mean thickness of Gangotri glacier's other tributaries ranges between 75.97 and 119.03 m. We compared with the earlier reported calculations (Fig. 8) of thickness along the Gangotri glacier and found that the average thickness is within the limit. The whole glacier ice volume from above methods is estimated as 42.47 km^3.

The present study gives an estimate of average ice thickness for Gangotri glacier using three methods as, 68, 92–101 and 125 m from slope dependent model, laminar flow model, and GlabTop model, respectively. Future work can include the use of Ground Penetrating Radar (GPR) for ice thickness measurement and validation of the ice thickness for part or whole glacier if used in air-based platforms. This can help to reduce uncertainty involved in glacier ice thickness estimation (Farinotti et al., 2017). Field survey using kinematic DGPS and repeat terrestrial photogrammetry can also be utilized to validate surface velocity of the glacier. Parameterization of the laminar flow model for density, scaling factor, creep factor, and basal velocity can be further studied for better results and improving the reliability of remote sensing based glacier velocity based glacier ice depth estimates.

Next, we estimated the thickness from velocity inputs and the laminar flow model (Fig. 9a–c). The glacier thickness is calculated from mean velocity from 1998 to 2014 (Fig. 9a), 2000 to 2001 (Fig. 9b), and 2018 to 2019 (Fig. 9c) periods. A 5–30% velocity fraction was considered

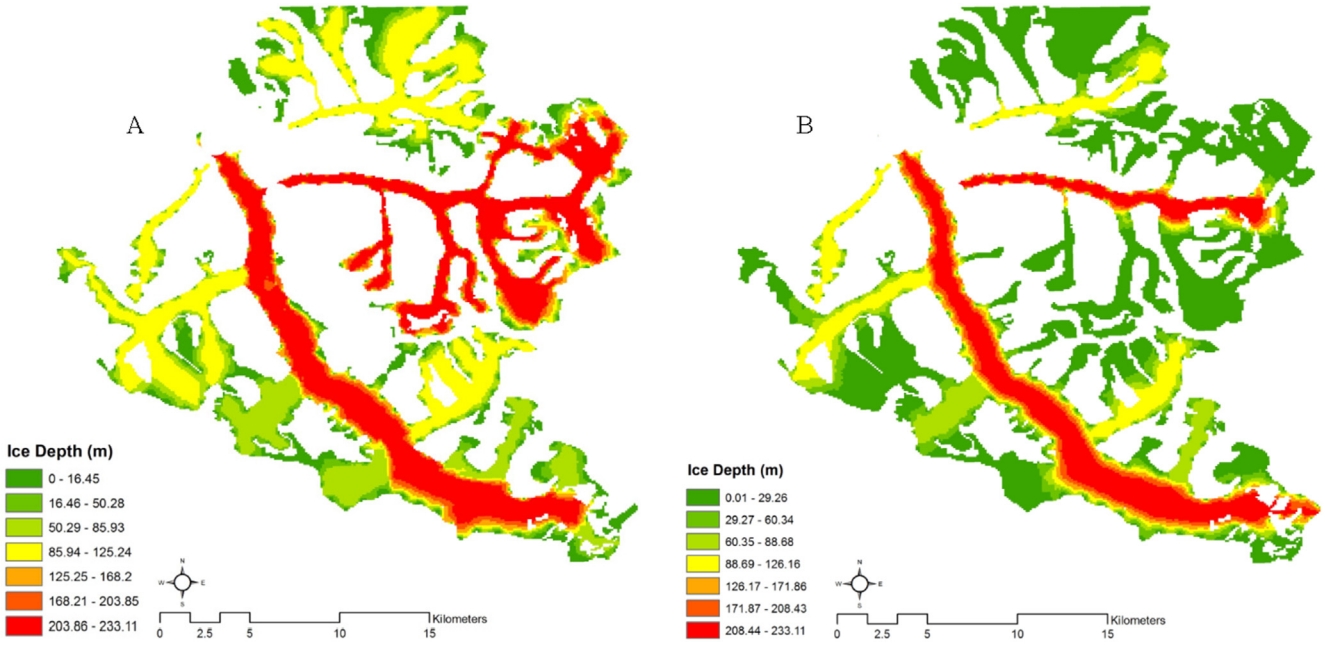

Fig. 7. Ice thickness for the Gangotri glacier. (a) Glacier Ice depth from GlabTop model and (b) same as (a) but for slope dependent equations.

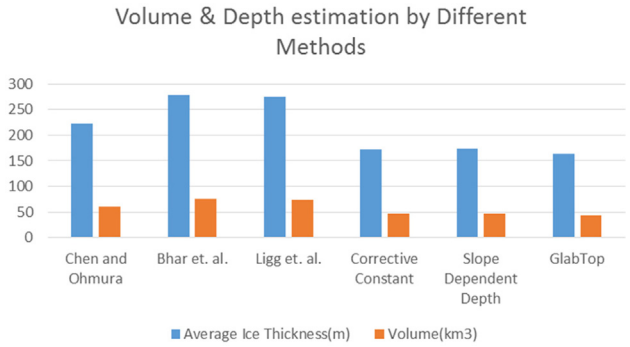

Fig. 8. Ice thickness estimated for various volume-area scaling and slope dependent models. y axis is average ice thickness (in meter – m) and average total volume calculated from the relation (km^3).

for laminar flow-based thickness estimation. We found varying ice thicknesses across different cross-sections along the Gangotri glacier, with maximum thickness at center of the glacier and minimum at the edges (Fig. 9). We observed an inverse relationship between ice thickness and velocity. The thickness from the laminar flow calculation is larger (20–400 m) for the Gangotri glacier. Further, the thickness at the glacier snout is small (24–62 m), whereas larger values were observed for the upper glacier (~607 m). The large values were observed for the 5% basal velocity (Fig. 9a & b). The ice thickness obtained from the analysis shows how the velocity variation changes the dynamics of the glacier. Therefore, glacier velocity at high spatial–temporal resolution is necessary to understand the current condition of the dynamic characteristics.

We obtained the average thickness from previous studies to understand the uncertainty. The uncertainty for ice thickness from the current study is 11.4%. The previous study used Landsat-7 based velocity and ASTER DEM to estimate thickness in the range of 15–540 m as reported by Gantayat et al. (2014). The differences in ice thickness may be due to the high-resolution velocity measurement and SRTM DEM (Farinotti et al., 2009a,b). Next, we validated the TLS and DGPS measurements at the snout. In 2014 fieldwork, more than 12 DGPS reading were taken. One DGPS reading at glacier snout top and one at the location of TLS gave relative height difference of 44.0 m. TLS was positioned near about 20 m above the snout ice on the right bank of the glacier, as it was not feasible to keep TLS exactly below or in front of snout due to danger of falling ice and high melt-water. Therefore, the total snout height is estimated at 64 m, which is close to our estimated ice thickness from TLS scan as well as from laminar flow based ice thickness model. The error in snout height estimated by TLS, DGPS and modeling methods can also be attributed to the different data source with high-resolution data such as IRS 1C/1D Pan Data and SRTM DEM based slope.

The TLS ice thickness at the Gangotri snout location (58–67 m) is validated with model ice thickness (~60 m). We found a correlation coefficient of 0.799 between the model results and observation (Fig. 10).

Finally, the elevation obtained from the TanDEM-X DEM (T3) was validated with observation during October 2012, which yielded a root mean square error of 8.3–11.32 m near the snout location. Consecutively the ice thickness estimated from TLS (64 m) near the snout during 2014 is approximately equal to the laminar flow-based ice thickness model (~60 m). The error in snout height estimated from the TLS, DGPS, and modeling methods can also be attributed to the different high-resolution data sets such as IRS 1C/1D, Pan Data, and SRTM DEM based slope.

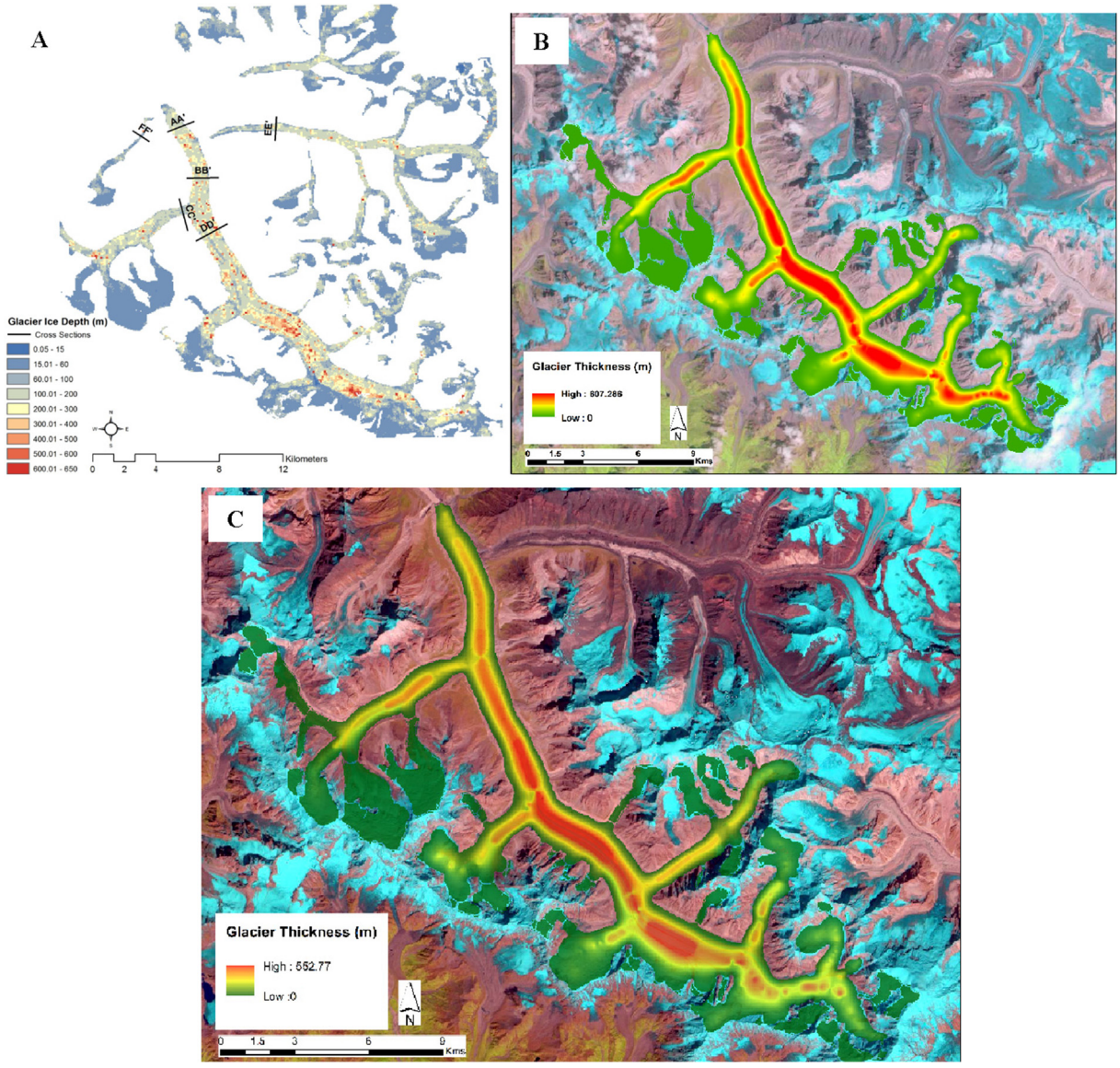

Fig. 9. Ice thickness estimation. (a) Gangotri glacier ice thickness from mean velocity during 1998–2014 period, (b) same as (a) but for the 2018–2019 period, and (c) same as (a) but for the 2000–2001 period. Here, standard colour composite image of 19 September 2018 is used as the background for b & c.

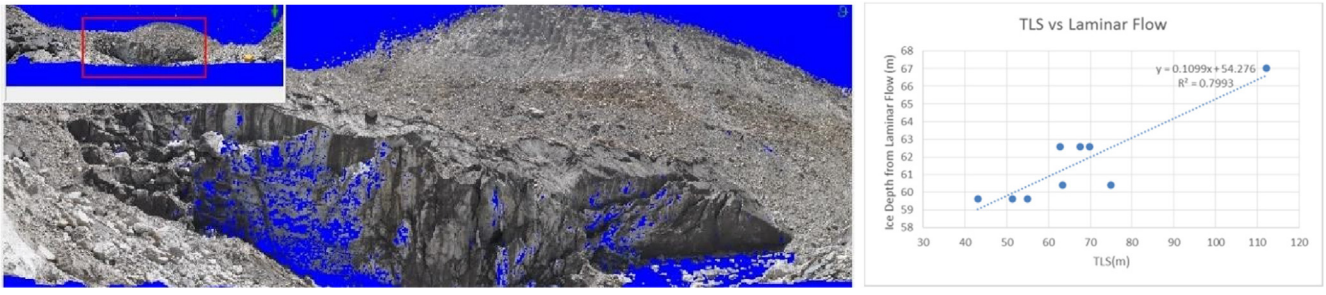

Fig. 10. Correlation between Terrestrial Laser Scanner (TLS) and Laminar Flow Model (LFM) at snout. The left panel shows the actual scan of snout in-situ observation during (15–17) September 2014.

4. Conclusions

A large-scale change in glacier dynamics is expected in the current climate scenarios. The Himalayan glacier in the future can be impacted due to the large seasonal temperature variation. The temperature increases above the long-term average are expected to modulate the glacier melt, snowfall, and velocity change within a season. Understanding the glacier dynamics is crucial for the overall Himalayan river basin management plans. Our analysis of various SAR datasets shows that glacier velocity can vary rapidly within a season and annually. It was noticed that the velocity of the glacier is decreasing over the period from 1998 to 2019. It was in the order of 24 m/year during 1998–2000, however, it decreased to around 15 m/year in the year 2014–15. Along with decreasing glacier surface velocity, it was observed that the mean glacier elevation over the main trunk region has reduced by around 5–10 m during the 2000–2014 period. The long-term negative change in thickness can be an indicator of glacier health deterioration. The change in glacier elevation and subsequent reduction in glacier velocity indicated the loss of glacier mass. It was further verified with glacier ice-thickness change analysis. However, our analysis shows that high-resolution velocity and elevation change estimation can improve the dynamic properties due to the scale of information. Our results show that the ice thickness is more accurately estimated from a high-resolution velocity. Further, the glacier dynamics over a season can contribute significantly to better understanding of glacio-hydrological processes. High-resolution TanDEM-X DEM and velocity estimation show that understanding the glacier dynamics within a season is crucial. Our results further highlight the use of combining high-resolution SAR, optical and In-situ datasets for a better understanding of the projected change in glacier dynamics. The current study with SAR data has shown that glacier velocity can be derived using DInSAR techniques for Himalayan glaciers. It will be an important scientific input to upcoming mission of NASA-ISRO SAR, NISAR (NISAR, 2015), as it will provide DInSAR data from S and L-band based sensors at every 12 days interval, and which will provide continuous and repeated information on glacier velocity covering all the seasons.

Declaration of Competing Interest

The authors declare that they have no known competing financial interests or personal relationships that could have appeared to influence the work reported in this paper.

Acknowledgements

Authors express their sincere thanks to former Directors of IIRS, Dr. YVN Krishnamurthy, Dr A Senthil Kumar for their constant support encouragement and all institutional facilities to complete this work. Thanks are also due for Head and faculty of Photogrammetry and Remote Sensing Department (PRSD) for providing and training of TLS and DGPS operations used in field survey, CMD IIRS and VSSC Trivandrum Engineers to provide solar panels and fuel cell based instrument charging systems during 2014 Gangotri field survey. Forest Department Uttarakhand and SASE Chandigarh are acknowledged for giving permission to visit Gangotri glacier and stay at Bhojbasa. The NRSC Data Centre (NDC) and USGS provided IRS, ERS 1, 2, Landsat and Sentinel-2 satellite data used in this study. Alaska SAR facility is acknowledged for providing the Sentinel-1 SAR satellite data. Dr. Praveen K. Thakur acknowledges TerraSAR-X data from DLR under TerraSAR-X Science Service project on, "Snow ice parameter retrieval with SAR (X-band) microwaveremote sensing", HYD0445; TanDEM-X by DLR under TanDEM-X Science Service project on, "Glacier dynamics studies in parts of Western Himalayas using TanDEM-X SAR data", NTI_INSA0461; and ALOS PALSAR-2 from JAXA under RA-4 project (PI No: 1408) under project "Hydrological parameter retrieval and glacier dynamics study with L-band SAR data". Thanks are due to Indian Institute of Science (IISC) Bangalore for sharing Himalayan Glacier Thickness Mapper (HIGTHIM) tool.

References

Anderson, R.S., 2004. Strong feedbacks between hydrology and sliding of a small alpine glacier. J. Geophys. Res. 109 (F3), 1–17. https://doi.org/10.1029/2004jf000120.

ASTER GDEM Validation Team, 2011. ASTER global digital elevation model version 2 summary of validation results, Tech. rep., http://www.jspacesystems.or.jp/ersdac/GDEM/ver2Validation/Summary_GDEM2_validation_report_finalpdf. Accessed on 20 July, 2017.

Azam, M.F., Kargel, J.S., Shea, J.M., Nepal, S., Haritashya, U.K., et al., 2021. Glaciohydrology of the Himalaya-Karakoram. Science 373 (6557), 1-17 pages, eabf3668. https://www.science.org/doi/10.1126/science.abf3668.

Azam, M.F., Wagnon, P., Berthier, E., Vincent, C., Fujita, K., Kargel, J. S., 2018. Review of the status and mass changes of Himalayan-Karakoram glaciers. J. Glaciol. 64, 61–74. https://doi.org/10.1017/jog.2017.86.

Azam, F.M., 2021. Need of integrated monitoring on reference glacier catchments for future water security in Himalaya. Water Security, 14 (100098), https://doi.org/10.1016/j.wasec.2021.100098.

Bahr, B., Meier, F., Peckham, S.D., 1997. The physical basis of glacier volume-area scaling perturbations in the ice mass balance rate of ice accumulation area at relatively high elevations low elevations (D < 0 on a yearly average), Volume-Size. J. Geophys. Res. 102 (B9), 20355–20362.

Bandyopadhyay, D., Singh, G., Kulkarni, A.V., 2019. Spatial distribution of decadal ice-thickness change and glacier stored water loss in the Upper Ganga basin, India during 2000–2014. Sci. Rep. 9 (1), 16730. https://doi.org/10.1038/s41598-019-53055-y.

Berthier, E., Arnaud, Y., Kumar, R., Ahmad, S., Wagnon, P., Chevallier, P., 2007. Remote sensing estimates of glacier mass balances in the Himachal Pradesh (Western Himalaya, India). Remote Sens. Environ. 108 (3), 327–338. https://doi.org/10.1016/j.rse.2006.11.017.

Bhambri, R., Bolch, T., Chaujar, R.K., 2012. Frontal recession of Gangotri Glacier, Garhwal Himalayas, from 1965 to 2006, measured through highresolution remote sensing data. Curr. Sci. 102 (3), 489–494. https://doi.org/10.5167/uzh-59630.

Bhattacharya, A., Arora, M.K., Sharma, M.L., 2012. Usefulness of synthetic aperture radar (SAR) interferometry for digital elevation model (DEM) generation and estimation of land surface displacement in Jharia coal field area. Geocarto Int. 27 (1), 57–77. https://doi.org/10.1080/10106049.2011.614358.

Bhushan, S., Syed, T.H., Kulkarni, A.V., Gantayat, P., Agarwal, V., 2017. Quantifying Changes in the Gangotri Glacier of Central Himalaya: Evidence for Increasing Mass Loss and Decreasing Velocity. IEEE J. Sel. Top. Appl. Earth Obs. Remote Sens. 10 (12), 5295–5306.

Bindschadler, R., Harrison, W.D., Raymond, C.F., Crosson, R., 1977. Geometry and dynamics of a surge-type glacier. J. Glaciol. 18, 181–194.

Bisht, S. M., Thakur P. K, Chouksey, A., Aggarwal, S.P., 2015. Ice Thickness Estimation using Geospatial Technology. In: Proceedings of 'HYDRO 2015 INTERNATIONAL', 20th International Conference on Hydraulics, Water Resources and River Engineering at IIT Roorkee, India, 17-19 December, 2015.

Bolch, T., Kulkarni, A., Kääb, A., Huggel, C., Paul, F., Cogley, J.G., Frey, H., Kargel, J.S., Fujita, K., Scheel, M., Bajracharya, S., Stoffel, M., 2012. The state and fate of Himalayan glaciers. Science 336 (6079), 310–314. https://doi.org/10.1126/science.121582.

Chen, J., Ohmura, A., 1990. Estimation of Alpine glacier water resources and their change since the 1870s. Hydrol. Mountainous Regions I, 127–135.

Clarke, G., Anslow, F., Jarosch, A., Radic, V., Menounos, B., Bolch, T., Berthier, E., 2013. Ice volume and subglacial topography for western Canadian glaciers from mass balance fields, thinning rates, and a bed stress model. J. Climate 26, 4282–4303. https://doi.org/10.1175/JCLI-D-12-00513.1.

Clarke, G.K.C., Berthier, E., Schoof, C.G., Jarosch, A.H., 2009. Neural networks applied to estimating subglacial topography and glacier volume. J. Climate 22 (8), 2146–2160. https://doi.org/10.1175/2008JCLI2572.1.

Costantini, M., 1998. A novel phase unwrapping method based on network programming. IEEE Trans. Geosci. Remote Sens. 36 (3), 813–821.

Cuffey, K.M., Paterson, W.S.B., 2010. The Physics of Glaciers Ed. 4. Elsevier, USA.

Dehecq, A., Gourmelen, N., Gardner, A.S., et al., 2019. Twenty-first century glacier slowdown driven by mass loss in High Mountain Asia. Nature Geosci. 12, 22–27. https://doi.org/10.1038/s41561-018-0271-9.

Detlev, K., Wessel B., Schwieger, V., 2010. Global Digital Elevation Model from TanDEM-X and the Calibration/Validation with worldwide kinematic GPS-Tracks. In the XXIV FIG International Congress, Facing the Challenges – Building the Capacity, Sydney, Australia, pp. 1-14, 11-16 April 2010.

Dhote, P.R., Thakur, P.K., Chouksey, A., Srivastav, S.K., Raghvendra, S., Rautela, P., Ranjan, R., Allen, S., Stoffel, M., Bisht, S., Negi, B.S., Aggarwal, S.P., Chauhan, P., 2021. Synergistic analysis of satellite, unmanned aerial vehicle, terrestrial laser scanner data and process-based modelling for understanding the dynamics and morphological changes around the snout of Gangotri Glacier, India. Geomorphology, 2021, 108005, ISSN 0169-555X, https://doi.org/10.1016/j.geomorph.2021.108005.

Farinotti, D., Huss, M., Bauder, A., Funk, M., 2009a. An estimate of the glacier ice volume in the Swiss Alps. Global Planet. Change 68 (3), 225–231. https://doi.org/10.1016/j.gloplacha.2009.05.004.

Farinotti, D., Huss, M., Bauder, A., Funk, M., Truffer, M., 2009b. A method to estimate the ice volume and ice-thickness distribution of alpine glaciers. J. Glaciol. 55 (191), 422–430. https://doi.org/10.3189/002214309788816759.

Farinotti, D., Brinkerhoff, D.J., Clarke, G.K.C., Fürst, J.J., Frey, H., Gantayat, P., Gillet-Chaulet, F., Girard, C., Huss, M., Leclercq, P.W., Linsbauer, A., Machguth, H., Martin, C., Maussion, F., Morlighem, M., Mosbeux, C., Pandit, A., Portmann, A., Rabatel, A., Andreassen, L.M., 2017. How accurate are estimates of glacier ice thickness? Results from ITMIX, the Ice Thickness Models Intercomparison experiment. Cryosphere 11 (2), 949–970. https://doi.org/10.5194/tc-11-949-2017.

Fountain, A.G., Walder, J.S., 1998. Water flow through temperate glaciers. Rev. Geophys. 36 (3), 299–328. https://doi.org/10.1029/97RG03579.

Frey, H., Machguth, H., Huss, M., Huggel, C., Bajracharya, S., Bolch, T., Kulkarni, A., Linsbauer, A., Salzmann, N., Stoffel, M., 2014. Estimating the volume of glaciers in the Himalayan-Karakoram region using different methods. Cryosphere 8 (6), 2313–2333. https://doi.org/10.5194/tc-8-2313-2014.

Fritz, T., Rossi, C., Yague-Martinez, N., Rodriguez-Gonzalez, F., Lachaise, M., Breit, H., 2011. Interferometric processing of TanDEM-X data. International Geoscience and Remote Sensing Symposium (IGARSS), July 2010, 2428–2431. https://doi.org/10.1109/IGARSS.2011.6049701.

Gantayat, P., Kulkarni, A.V., Srinivasan, J., 2014. Estimation of ice thickness using surface velocities and slope: Case study at Gangotri Glacier. India. Journal of Glaciology 60 (220), 277–282. https://doi.org/10.3189/2014JoG13J078.

Glen, J.W., 1955. The creep of polycrystalline ice. Proc. R. Soc. Lond. Ser. A. Math. Phys. Sci. 228 (1175), 519–538.

Gruber, A., Wessel, B., Huber, M., 2009. TanDEM-X DEM calibration: Correction of systematic DEM errors by block adjustment. International Geoscience and Remote Sensing Symposium (IGARSS) 2, 761–764. https://doi.org/10.1109/IGARSS.2009.5418202.

Gudmundsson, G.H., Bassi, A., Vonmoos, M., Bauder, A., Fischer, U.H., Funk, M., 2000. High-resolution measurements of spatial and temporal variations in surface velocities of Unteraargletscher, Bernese Alps, Switzerland. Ann. Glaciol. 31 (1), 63–68. https://doi.org/10.3189/172756400781820156.

Haeberli, W., Hölzle, M., 1995. Application of inventory data for estimating characteristics of and regional climate-change effects on mountain glaciers: a pilot study with the European Alps. Ann. Glaciol. 21, 206–212.

Hanssen, R.F., 2001. Radar interferometry: data interpretation and error analysis. ISSN: 9780792369455, Vol. 2: Springer, 2001.

Huber, M., Wessel, B., Kosmann, D., Felbier, A., Schwieger, V., Habermeyer, M., Wendleder, A., Roth, A., 2009. Ensuring globally the TanDEM-X height accuracy: Analysis of the reference data sets ICESat, SRTM and KGPS-tracks. International Geoscience and Remote Sensing Symposium (IGARSS), 2, II-769-II–772. https://doi.org/10.1109/IGARSS.2009.5418204.

Huda, M.B., Kumar, R., Lone, M.A., Tantray, F.A., 2021. Climate change and water resources of Himalayan region—review of impacts and implication. Arab J Geosci 14, 1088. https://doi.org/10.1007/s12517-021-07438-z.

Huss, M., Farinotti, D., 2012. Distributed ice thickness and volume of all glaciers around the globe. J. Geophys. Res., 117, F04010, 2012, 117 (June), 1–10. https://doi.org/10.1029/2012JF002523.

Huss, M., Farinotti, D., Bauder, A., Funk, M., 2008. Modelling runoff from highly glacierized alpine drainage basins in a changing climate. Hydrol. Process. 22 (19), 3888–3902. https://doi.org/10.1002/hyp.7055.

Immerzeel, W.W., Van Beek, L.P.H., Bierkens, M.F.P., 2010. Climate change will affect the Asian water towers. Science 328 (5984), 1382–1385. https://doi.org/10.1126/science.1183188.

Immerzeel, W.W., Lutz, A.F., Andrade, M., Bahl, A., Biemans, H., Bolch, T., et al., 2020. Importance and vulnerability of the world's water towers. Nature 577, 364–369. https://doi.org/10.1038/s41586-019-1822-y.

Jain, S.K., 2008. Impact of retreat of Gangotri glacier on the flow of Ganga River. Curr. Sci. 95 (8), 1012–1014.

Joel, H.T., Humphrey, N.F., Pfeffer, W.T., Lazar, B., 2007. Two modes of accelerated glacier sliding related to water. Geophys. Res. Lett. 34 (12), L12503.

Joughin, I., Smith, B.E., Abdalati, W., 2010. Glaciological advances made with interferometric synthetic aperture radar. J. Glaciol. 56 (200), 1026–1042. https://doi.org/10.3189/002214311796406158.

Just, D., Balmer, R., 1994. Phase statistics of interferograms with applications to synthetic aperture radar. Appl. Opt. 33, 4361–4368.

Karimi, N., Farokhnia, A., Karimi, L., Eftekhari, M., Ghalkhani, H., 2012. Combining optical and thermal remote sensing data for mapping debris-covered glaciers (Alamkouh Glaciers, Iran). Cold Reg. Sci. Technol. 71 (10), 73–83. https://doi.org/10.1016/j.coldregions.2011.10.004.

Kaser, G., Großhauser, M., Marzeion, B., 2010. Contribution potential of glaciers to water availability in different climate regimes. Proc. Natl. Acad. Sci. 107 (47), 20223–20227. https://doi.org/10.1073/PNAS.1008162107.

Khalsa, S.J.S., Dyurgerov, M.B., Khromova, T., Raup, B.H., Barry, R. G., 2004. Space-based mapping of glacier changes using ASTER and GIS tools. IEEE Trans. Geosci. Remote Sens. 42 (10), 2177–2183. https://doi.org/10.1109/TGRS.2004.834636.

Krieger, G., Moreira, A., Fiedler, H., Hajnsek, I., Werner, M., Younis, M., Zink, M., 2007. TanDEM-X: A satellite formation for high-resolution SAR interferometry. IEEE Transactions on Geoscience and Remote Sensing, 45(11), 3317-3341, Nov. 2007, https://doi.org/10.1109/TGRS.2007.900693.

Kulkarni, A.V., Bahuguna, I.M., Rathore, B.P., Singh, S.K., Randhawa, S.S., Sood, R.K., Dhar, S., 2007. Glacial retreat in Himalaya using Indian remote sensing satellite data. Curr. Sci. 92 (1), 69–74.

Kumar, K., Dumka, R.K., Miral, M.S., Satyal, G.S., Pant, M., 2008. Estimation of retreat rate of Gangotri glacier using rapid static and kinematic GPS survey. Curr. Sci. 94 (2), 258–262.

Kumar, V., Venkataraman, G., Rao, Y. S., 2009. SAR interferometry and speckle tracking approach for glacier velocity estimation using ERS-1/2 and TerraSAR-X spotlight high resolution data. International Geoscience and Remote Sensing Symposium (IGARSS), 5, V-332-V–335. https://doi.org/10.1109/IGARSS.2009.5417663.

Kumar, R., Kumar, R., Singh, S., et al., 2018. Dynamics of suspended sediment load with respect to summer discharge and temperatures in Shaune Garang glacierized catchment, Western Himalaya. Acta Geophys. 66, 1109–1120. https://doi.org/10.1007/s11600-018-0184-4.

Kumar, V., Venkataraman, G., Høgda, K.A., Larsen, Y., 2013. Estimation and validation of glacier surface motion in the North Western Himalayas using high-resolution SAR intensity tracking. Int. J. Remote Sens. 34 (15), 5518–5529. https://doi.org/10.1080/01431161.2013.792965.

Leprince, S., Barbot, S., Ayoub, F., Avouac, J.P., 2007. Automatic and precise orthorectification, coregistration, and subpixel correlation of satellite images, application to ground deformation measurements. IEEE Trans. Geosci. Remote Sens. 45 (6), 1529–1558. https://doi.org/10.1109/TGRS.2006.888937.

Li, S., Benson, C., Gens, R., Lingle, C., 2008. Motion patterns of Nabesna Glacier (Alaska) revealed by interferometric SAR techniques. Remote Sens. Environ. 112 (9), 3628–3638. https://doi.org/10.1016/j.rse.2008.05.015.

Li, H., Ng, F., Li, Z., Qin, D., Cheng, G., 2011. An extended "perfect-plasticity" method for estimating ice thickness along the flow line of mountain glaciers. J. Geophys. Res., Vol. 117, F01020, 2012, 117(May 2011), 1–11. https://doi.org/10.1029/2011JF002104.

LIGG, WECS, and NEA (1988). Report on first expedition to glaciers and glacier lakes in the Pumqu (Arun) and Poiqu (Bhote-Sun Kosi) river basins, Xizang (Tibet), China, Science Press, Beijing, China, 1988.

Linsbauer, A., Paul, F., Hoelzle, M., Frey, H., Haeberli, W., 2009. The Swiss Alps without glaciers a GIS-based modelling approach for reconstruction of glacier beds. Proc. Geomorphomet. 2009, 243–247. https://doi.org/10.5167/uzh-27834.

Anderson, B., Mackintosh, A., 2006. Temperature change is the major driver of late-glacial and Holocene glacier fluctuations in New Zealand. Geology 34, 121–124.

Mathieu, R., Chinn, T., Fitzharris, B., 2009. Detecting the equilibrium-line altitudes of New Zealand glaciers using ASTER satellite images. N. Z. J. Geol. Geophys. 52 (3), 209–222. https://doi.org/10.1080/00288300909509887.

McNabb, R.W., Hock, R., O'Neel, S., Rasmussen, L.A., Ahn, Y., Braun, M., Conway, H., Herreid, S., Joughin, I., Pfeffer, W.T., Smith, B.E., Truffer, M., 2012. Using surface velocities to calculate ice thickness and bed topography: A case study at Columbia Glacier, Alaska, USA. J. Glaciol. 58 (212), 1151–1164. https://doi.org/10.3189/2012JoG11J249.

Natural Resources Canada NRC, 1995. GPS Positioning Guide. Published by authority of Natural Resources Canada, Geomatics Canada, Geodetic Survey Division, Information Services, 615 Booth Street, Ottawa, Ontario, K1A 0E9, Cat. No. M52-74/1995E, ISBN 0-660-15917-1, Third printing July 1995, 123 pages.

Negi, H.S., Thakur, N.K., Ganju, A., Snehmani,, 2012. Monitoring of Gangotri glacier using remote sensing and ground observations. J. Earth Syst. Sci. 121 (4), 855–866. https://doi.org/10.1007/s12040-012-0199-1.

NISAR, 2015. Applications Workshop Report, "Applications Community Suggestions for developing an application plan," https://nisar.jpl.nasa.gov/files/nisar/2015_NISAR_Application_Workshop_Report_20160926.pdf, October 13-15, 2015.

Nuth, C., Kääb, A., 2011. Co-registration and bias corrections of satellite elevation data sets for quantifying glacier thickness change. Cryosphere 5 (1), 271–290. https://doi.org/10.5194/tc-5-271-2011.

Orr, A., Ahmad, B., Alam, U., Appadurai, A., Bharucha, Z.P., Biemans, H., et al., 2022. Knowledge Priorities on Climate Change and Water in the Upper Indus Basin: A Horizon Scanning Exercise to Identify the Top 100 Research Questions in Social and Natural Sciences. Earth's Future. https://doi.org/10.1029/2021EF002619.

Pandey, P., Manickam, S., Bhattacharya, A., Singh, G., Venkataraman, G., Ray, P.K.C., 2016. Mass change of Gangotri glacier based on TanDEM-X measurements. IEEE International Geoscience and Remote Sensing Symposium (IGARSS) 2016, 6168–6170. https://doi.org/10.1109/IGARSS.2016.7730611.

Pandit, A., Ramsankaran, R., Rao, Y.S., 2014. Generation and Validation of the Interferometric SAR DEMs from TanDEM-X data for Gangotri and Hamtah Glaciers of Indian Himalayas. Procedia Technol. 16 (2014), 793–805. https://doi.org/10.1016/j.protcy.2014.10.029.

Paul, F., Linsbauer, A., 2012. Modeling of glacier bed topography from glacier outlines, central branch lines, and a DEM. Int. J. Geogr. Inf. Sci. 26 (7), 1173–1190. https://doi.org/10.1080/13658816.2011.627859.

Racoviteanu, A.E., Manley, W.F., Arnaud, Y., Williams, M.W., 2007. Evaluating digital elevation models for glaciologic applications: An example from Nevado Coropuna, Peruvian Andes. Global Planet. Change 59 (1–4), 110–125. https://doi.org/10.1016/j.gloplacha.2006.11.036.

Rizzoli, P., Martone, M., Gonzalez, C., Wecklich, C., et al., 2017. Generation and performance assessment of the global TanDEM-X digital elevation model. ISPRS J. Photogramm. Remote Sens. 132, 119–139. https://doi.org/10.1016/j.isprsjprs.2017.08.008.

Rodríguez, E., Morris, C.S., Belz, J.E., 2006. A global assessment of the SRTM performance. Photogramm. Eng. Remote Sens. 72 (3), 249–260. https://doi.org/10.14358/PERS.72.3.249.

Saraswat, P., Syed, T.H., Famiglietti, J.S., Fielding, E.J., Crippen, R., Gupta, N., Saraswat, P., Syed, T.H., Famiglietti, J.S., Fielding, E.J., 2013. Recent changes in the snout position and surface velocity of Gangotri glacier observed from space. Int. J. Remote Sens. 34 (24), 8653–8668. https://doi.org/10.1080/01431161.2013.845923.

Satyabala, S.P., 2016. Spatiotemporal variations in surface velocity of the Gangotri glacier, Garhwal Himalaya, India: Study using synthetic aperture radar data. Remote Sens. Environ. 181 (2016), 151–161. https://doi.org/10.1016/j.rse.2016.03.042.

Scherler, D., Leprince, S., Strecker, M.R., 2008. Glacier-surface velocities in alpine terrain from optical satellite imagery-Accuracy improvement and quality assessment. Remote Sens. Environ. 112 (10), 3806–3819. https://doi.org/10.1016/j.rse.2008.05.018.

Schneevoigt, N.J., Sund, M., Bogren, W., Kääb, A., Weydahl, D.J., 2012. Glacier displacement on Comfortlessbreen, Svalbard, using 2-pass differential SAR interferometry (DInSAR) with a digital elevation

model. Polar Rec. 48 (1), 17–25. https://doi.org/10.1017/S0032247411000453.

Singh, P., Haritashya, U.K., Kumar, N., Singh, Y., 2006. Hydrological characteristics of the Gangotri glacier, central Himalayas, India. J. Hydrol. 327 (1), 55–67. https://doi.org/10.1016/j.jhydrol.2005.11.060.

Singh, P., Haritashya, U.K., Kumar, N., 2007. Meteorological study for Gangotri Glacier and its comparison with other high altitude meteorological stations in central Himalayan region. Nord. Hydrol. 38 (1), 59–77. https://doi.org/10.2166/nh.2007.028.

Small, D., Werner, C., Nuesch, D., 1993. Baseline modelling for ERS-1 SAR interferometry. International Geoscience and Remote Sensing Symposium (IGARSS) 3 (1), 1204–1206. https://doi.org/10.1109/igarss.1993.322661.

Strozzi, T., Wiesmann, A., Sharov, A., Kouraev, A., Wegmuller, U., Werner, C., 2006. Capabilities of L-band SAR data for Arctic glacier motion estimation. International Geoscience and Remote Sensing Symposium (IGARSS), October 1994, 3799–3802. https://doi.org/10.1109/IGARSS.2006.978.

Strozzi, T., Wegmuller, U., Matzler, C., 1999. Mapping wet snow covers with SAR interferometry. Int. J. Remote Sens. 20 (12), 2395–2403. https://doi.org/10.1080/014311699212083.

Strozzi, T., Luckman, A., Murray, T., Wegmüller, U., Werner, C.L., 2002. Glacier Motion Estimation Using SAR Offset-Tracking Procedures. IEEE Trans. Geosci. Remote Sens. 40 (11), 2384–2391. https://doi.org/10.1109/TGRS.2002.805079.

Thakur, P. K., Dixit, A., Chouksey, A., Aggarwal, S. P., & Kumar, A. S., 2016. Ice sheet features identification, glacier velocity estimation, and glacier zones classification using high-resolution optical and SAR data. Land Surface and Cryosphere Remote Sensing III, 9877 (May 2016), 987719. https://doi.org/10.1117/12.2224027.

Thakur, P.K., Garg, V., Nikam, B.R., Chouksey, A., Aggarwal, S.P., Dhote, P.R., 2017. Cryospheric Studies in Indian Himalayan and Polar Region: Current Status, Advances and Future Prospects of Remote Sensing. Proc. Natl. Acad. Sci., India Sect. A: Phys. Sci. 87 (4), 593–616. https://doi.org/10.1007/s40010-017-0437-7.

Thakur, P.K., Garg, V., Nikam, B.R., Singh, S., Jasmine, Chouksey, A., Dhote, P.R., Aggarwal, S.P., Chauhan, P., Kumar, A.S., 2018. Snow Cover and Glacier Dynamics Study Using C-and L-Band SAR Datasets in Parts of North West Himalaya. Int. Arch. Photogramm. Remote Sens. Spatial Inf. Sci. XLII-5, 375–382. https://doi.org/10.5194/isprs-archives-XLII-5-375-2018.

Wangensteen, B., Weydahl, D.J., Hagen, J.O., 2005. Mapping glacier velocities on Svalbard using ERS tandem DInSAR data. Nor. Geogr. Tidsskr. 59 (4), 276–285. https://doi.org/10.1080/00291950500375500.

Wegmüller, U., Werner, C., 1997. Gamma SAR processor and interferometry software. ESA SP, 1687–1692.

Wells, D.E., Beck, N., Delikaraoglou, D., Kleusberg, A., Krakiwsky, E.J., Lachapelle, G., Langley, R.B., Nakiboglu, M., Schwarz, K.P., Tranquilla, J.M., 1999. Guide to GPS positioning. Geodesy. Geomatics Lecture Notes 58.

Wessels, R.L., Kargel, J.S., Kieffer, H.H., 2002. ASTER measurement of supraglacial lakes in the Mount Everest region of the Himalaya. Ann. Glaciol. 34, 399–408. https://doi.org/10.3189/172756402781817545.

Willis, I.C., 1995. Intra-annual variations in glacier motion: a review. Prog. Phys. Geogr. 19 (1), 61–106.

Wood, L.R., Neumann, K., Nicholson, K.N., Bird, B.W., Dowling, C.B., Sharma, S., 2020. Melting Himalayan Glaciers Threaten Domestic Water Resources in the Mount Everest Region. Nepal. Front. Earth Sci. 8, 128. https://doi.org/10.3389/feart.2020.00128.